Mine Water and the Environment (2022) 41:126–142
https://doi.org/10.1007/s10230-021-00810-1

TECHNICAL ARTICLE

Identification of Mine Water Sources Based on the Spatial and Chemical Characteristics of Bedrock Brines: A Case Study of the Xinli Gold Mine

Xueliang Duan[1,2,3] · Fengshan Ma[1,2] · Hongyu Gu[4] · Jie Guo[1,2] · Haijun Zhao[1,2] · Guowei Liu[1,2,3] · Shuaiqi Liu[1,2,3]

Received: 29 May 2020 / Accepted: 27 July 2021 / Published online: 10 August 2021

Abstract

Water inrush caused by mining below the seafloor is extremely harmful to mine production. Identifying the sources of mine water can help guide mine water management and sustainable mine development. Saline brines were known to be entering the Xinli Mine, a portion of which lies beneath Laizhou Bay, Shandong Province, China. Preliminary classification of the bedrock brines was determined using hydrochemical analysis and the spatial position of the brines. Four bedrock brine types were identified: shallow, middle, middle high-salinity, and deep. The study area was divided into three levels (shallow, middle, and deep) according to the spatial distribution of the brines. Hierarchical-multi-index analysis (HMIA) was used, along with five pairs of chemical indicators (Cl, $\delta^{18}O$, Mg, Ca, SO_4, Na), to identify the mixing lines for each level. A ternary hybrid model was used to calculate the mixing ratio of mine water from different sources in the shallow sublevels. The bedrock brine classification and water source identification were evaluated by analysis of brine genesis and mixing ratio deviation, respectively. The mixed modes of mine water in the shallow and middle sublevels were seawater-saline water-shallow brine and seawater-saline water-middle brine, respectively. The mixed modes in the deep sublevels were seawater-saline water-deep brine and seawater-saline water-middle brine with a transition between these two modes. Previous studies classified bedrock brine as only one category, and using the mixing ratio greatly improved accuracy. The average proportion of seawater in the mine water has increased over time, but the rate of increased has slowed. In the shallow sublevels, the proportion of seawater in the − 105 m sublevel was higher than that in the − 135 m sublevel, but the difference has decreased every year, indicating that the seawater mainly infiltrates by vertical recharge. The mine water samples from the footwall and in the middle of the − 105 m sublevel were nearly 50% seawater, while the mine water sites on the hanging wall had a relatively low seawater proportion, indicating that the water-conducting fractures were mainly in the footwall.

Keywords Water inrush · Subsea mining · Water source identification

✉ Fengshan Ma
fsma@mail.iggcas.ac.cn

✉ Hongyu Gu
xy0909040129@126.com

Xueliang Duan
13051876966@163.com

Jie Guo
guojie@mail.iggcas.ac.cn

Haijun Zhao
zhaohaijun@mail.iggcas.ac.cn

Guowei Liu
l1014893489@163.com

Shuaiqi Liu
liushuaiqi@mails.iggcas.ac.cn

[1] Key Laboratory of Shale Gas and Geoengineering, Institute of Geology and Geophysics, Chinese Academy of Sciences, Beijing 100029, China

[2] Institutions of Earth Science, Chinese Academy of Sciences, Beijing 100029, China

[3] University of Chinese Academy of Sciences, Beijing 100049, China

[4] Chengdu Center, China Geological Survey, Chengdu 610081, China

Introduction

Mine water inrush has always been a difficult problem for mine development (Dong et al. 2021; Li et al. 2018; Wu et al. 2017). Because land resources are becoming depleted and the demand for mineral resources is increasing, mineral deposits below the seafloor are being targeted (Chung 1996; Rona 2003). These deposits are more dangerous and difficult to mine than land deposits, especially because of the higher potential for seawater infiltration and challenging inrush issues (Li 2018; Liu et al. 2012; Sui and Xu 2013). The Xinli gold deposit is the first such metal deposit in China to be mined. Some of the mine's underground workings are in rocks below the sea floor at a depth of ≈ 100 to 400 m below sea level. Water inrush during mining is becoming increasingly serious and there have been several water inrush accidents that have severely affected the safety of the mine and its workers (Li et al. 2013; Liu et al. 2018). The mine water inflow is associated with fractures and faults. However, it is difficult to directly study the distribution and formation of fractures and faults in an underground mine. Therefore, water sources are identified using isotopic and hydrochemical evaluation of water samples to guide mine water management and enhance mine safety.

Recent publications have contributed to the identification of mine water inrush sources in coal and other mines (Dong et al. 2019; Jiang et al. 2021; Zhang and Yao 2020). At present, two primary methods are used for water source identification. The first uses a comprehensive analysis of hydrochemistry and isotopes (Fan et al. 2016; Mauryaa et al. 2019; Yang et al. 2020) focusing on major ions and stable isotopes. This method is straightforward, but because it uses only a few indicators, it does not present complete information about the water sample (Guo et al. 2015; Li et al. 2016). The second method is based on multivariate statistical analysis, of which PCA is the most commonly used (Duan et al. 2019a; Gu et al. 2017, 2018a). In this method, several main chemical components of the water samples are identified by dimensionality reduction (or dimension reduction) of the water chemistry data (Laaksoharju et al. 1999; Peng et al. 2015). The main components can replace the numerous original indicators, which simplify the identification process. All water sample constituents are considered. However, including non-conservative indicators can affect the accuracy of the analysis. In addition, some key characteristics of the indicators may be "neutralized" during the dimension reduction process and potentially cause different water sources to not be distinguished. The main components are based on a weighted average of all indicators and this weakens the impact of the critical indicator.

Ma et al. (2015) determined the mine water end members in the Xinli gold mine using comprehensive analysis of geochemistry and stable isotopes, and their results showed that the mine water was composed of seawater, bedrock brine, and rainwater. Li et al. (2017) used the maximum likelihood method based on PCA to understand mine water evolution. Li et al. (2014) applied the cluster analysis method to assess the connectivity between the underground workings and overlying seawater. Peng et al. (2015) studied the laws of motion and evolution of the groundwater system using combined FCM (Fuzzy C-Means: a clustering algorithm based on fuzzy theory) and PCA methods (Güler and Thyne 2004; Güler et al. 2012). Yan et al. (2020) used the Bayesian model based on Markov chain Monte Carlo analysis to identify the mine water sources.

These researchers have contributed to mine water source identification in the Xinli gold mine. However, due to the time and regional scale of their studies, they did not characterize the composition of the bedrock brine in the study area. The brine end member was determined by selecting the extreme value in the isotope and ion correlation diagram (Gu et al. 2018b). However, when there are various brines, the actual brine end member reflected by some indicators might not have an extreme value and the brine with an extreme value is not necessarily the actual end member. Also, some researchers characterized the chemistry of the mine water using multivariate statistical analysis based on the Euclidean distance theory, which could ignore the chemical characteristics of some indicators (Liu et al. 2019, 2020). Adding to the complexity is the hydrogeologic characteristics of the study area, which includes several potential water sources (seawater, freshwater, Quaternary saline water, and bedrock brine). In addition, there are a variety of bedrock brines. Therefore, if traditional methods are used, the result will not reflect the actual complex situation (Gao et al. 2015; Su et al. 2011).

Calculating changes in the mixing ratios of different water sources in mine water is an important method for determining the risk of mine water inrush, and the calculation of mixing ratios requires an accurate identification of water sources. Previous studies classified bedrock brine as one category. In this study, the brine was divided into four categories, which laid the foundation for accurate identification of water sources and improved the accuracy of mixing ratio calculations. The objectives of this study was to distinguish the types of underground bedrock brines, identify the water sources, and calculate the mixing ratios of source waters contributing to mine water in the Xinli gold mine.

Study Area

Geological Conditions

The Xinli gold mine is located in the coastal area of Laizhou Bay in Shandong Province (Fig. 1). The terrain has low

topographic relief with an elevation of 1.2–4.3 m a.m.s.l. (meters above mean sea level). Bohai sea level is the lowest erosion base in this area, and all deposits are buried below it. The Xinli gold deposit is located in the north-central of the metallogenic belt of the Sanshandao fault area (Fig. 1a). The northern portion is adjacent to the Sanshandao gold deposit, and it is 5 km from the Cangshang gold deposit to the south. The fault zone partially outcrops at the surface and is mostly covered by Quaternary sediments. The general strike of the fault is NE40° and NE70–80° locally, with a dip of SE∠42–75°. The major fracture plane shows little undulation and is considered a compressional torsional fracture.

Fault F1 is part of the Sanshandao fault zone and is the ore-controlling structure of the Xinli gold deposit (Fig. 1b). The average attitude is NE62°/SE∠46°. The fault alteration zone is mainly composed of beresitized granite, cataclastic granite, and beresitized cataclasite. Other rock masses mainly consist of monzogranite and metagabbro. The ore body is located between 0 and 30 m below the major fracture plane, with an average thickness of 20–30 m, and a deposit

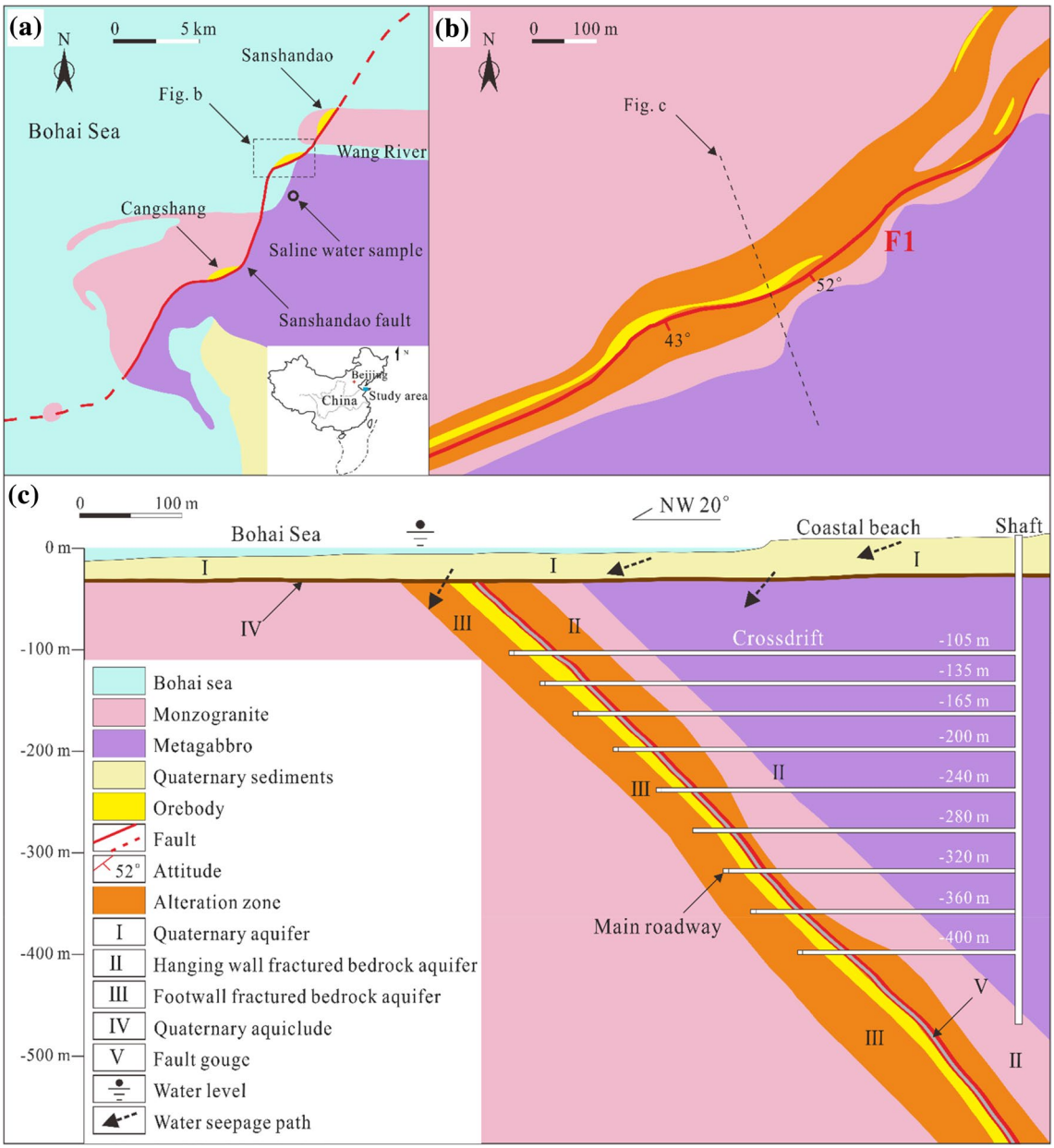

Fig. 1 **a** Simplified plan view geological map showing the Sanshandao fault and other features. **b** Close-up geological map of the Xinli gold deposit area showing the fault and the cross-section location. **c** Cross-section showing the fault, geology and hydrogeologic features, and the underground workings of the Xinli gold deposit

elevation of − 50 to − 600 m. The southwest corner of the ore body and the shallow ore are located below the seafloor (Chen et al. 2019; Peng et al. 2011).

Hydrologic Conditions

The surface water system in the mining area is the Wang River, but due to the regional dry climate and low precipitation, the river only flows during the rainy season (July and August) when there is a small amount of water in the river. Therefore, it has a minor effect on groundwater in the study area. The main surface water body in the area is the Bohai Sea, and most of the mine tunnels are located under the sea floor.

The groundwater system in the study area includes a Quaternary aquifer, a hanging wall fractured bedrock aquifer, a footwall fractured bedrock aquifer, a Quaternary aquiclude, and the fault gouge impermeable layer, which were represented by I, II, III, IV, and V, respectively (see Fig. 1c). Layers I, II, and III are aquifers and layers IV and V are aquifuges (Li et al. 2014a).

The aquifer system can be divided into two parts by the Quaternary aquiclude at the base of the Quaternary sediments. The first part is the Quaternary aquifer, which is located above this aquiclude. This aquifer is distributed in the shallow layer of the study area; the southeast side outcrops at the surface, and the western and northern sides are covered by the Bohai Sea. The aquifer is about 40 m thick and consists of coarse sand, sandy gravel, silty clay, etc. It has poor regularity and continuity, and large changes in permeability and water abundance. In general, this aquifer is very permeable and has a close hydraulic connection with the overlying seawater.

The second part is the fractured bedrock aquifer system, which is located stratigraphically below the Quaternary aquiclude. The bedrock aquifer can be divided into two parts (hanging wall fractured bedrock aquifer and footwall fractured bedrock aquifer) separated by the impermeable layer in the middle of F1. The hanging wall fractured bedrock aquifer is located in the hanging wall of the fault alteration belt of F1. It is distributed along F1, and its inclined depth is greater than 600 m. It is composed of beresitized granite, cataclastic granite, and metagabbro and is overlain by the Quaternary aquifer system, which is about 40 m thick. The permeability and water abundance of this aquifer are low. The footwall fractured bedrock aquifer is located in the footwall of F1 and is distributed along the lower part of the fracture plane with an inclined depth of 800 m and a horizontal width of 20–100 m. It consists of beresitized granite, cataclastic granite, and beresitized cataclasite. The fissures in the rock are not well developed, the permeability is low, and it is close to the impermeable layer. The ore body is located in this aquifer whose groundwater is the deposit's direct water source.

The aquifuge in this area includes the Quaternary aquiclude and the impermeable fault gouge layer. The Quaternary aquiclude at the base of the Quaternary sediments is located between the Quaternary aquifer and the bedrock. This layer is continuous throughout the study area. It is 0.8–10 m thick and composed of sandy and silty clay. This layer is distributed horizontally along the bedrock, and its structure is relatively dense (the clay content is high and stable); thus, it is impermeable. The Quaternary aquiclude separates the groundwater in the Quaternary aquifer from the bedrock fissure water system so there is no direct hydraulic connection, which is beneficial to the exploitation of the deposit. The fault gouge impermeable layer is distributed between the aquifers of the hanging wall and footwall. It is composed of fault gouge, mylonite, and cataclastic granite; the main marker bed is the black, dark-grey fault gouge, which is generally 1–10 cm thick, and has continuous distribution and very low permeability. The boundaries of the impermeable layer on both sides of the fault gouge are irregular and its width is generally 10–20 m. This impermeable layer largely prevents a hydraulic connection between the groundwater in the hanging wall and footwall (Zhao et al. 2012).

In general, the main water-bearing stratum of the mine area is the fractured bedrock aquifer, which has an uneven thickness and weak water abundance. However, the ore body is located below the Quaternary aquifer and Bohai Sea. Although the Quaternary aquiclude and the impermeable layer in the middle of F1 are natural hydrologic barriers, they have become more fractured by blasting and mine excavation, for example, by excavation of the cross drift that connects the shaft and the main underground roadway. Therefore, groundwater from the Quaternary aquifer and seawater infiltration pose a threat to deposit exploitation.

Methods

Sample Collection and Analysis

The water samples collected were divided into two categories. One was mine water from the underground roadways. Some of these samples were composed of or influenced by bedrock brines that originated from ancient seawater that experienced evaporation and concentration with high total dissolved solids (TDS generally > 50 g/L). The other sample category was seawater, freshwater, and Quaternary aquifer saline water (saline water for short). The freshwater was from the Wang River, while the saline water is groundwater in the Quaternary aquifer, which is supplied by seawater and freshwater and has undergone evaporation (Ma et al. 2007). Figure 2 shows the distribution and

locations of the underground roadways and water sampling sites.

As shown in Fig. 2a, most of the underground roadways are located in the northeast portion of the mine area, except for the − 165 m sublevel, which extends to the southwest of the mine area. Figure 2b shows the location of the sampling sites in various sublevels of the mine. Figure 2c shows the location of the sampling sites in the − 105 m sublevel. Most of the sampling sites were in the main underground roadway that parallels the orebody, and some sampling sites were in the branch roadways that cross the orebody, such as sampling sites 105-7, -11, -17, and -18, which are located in the hanging wall of F1.

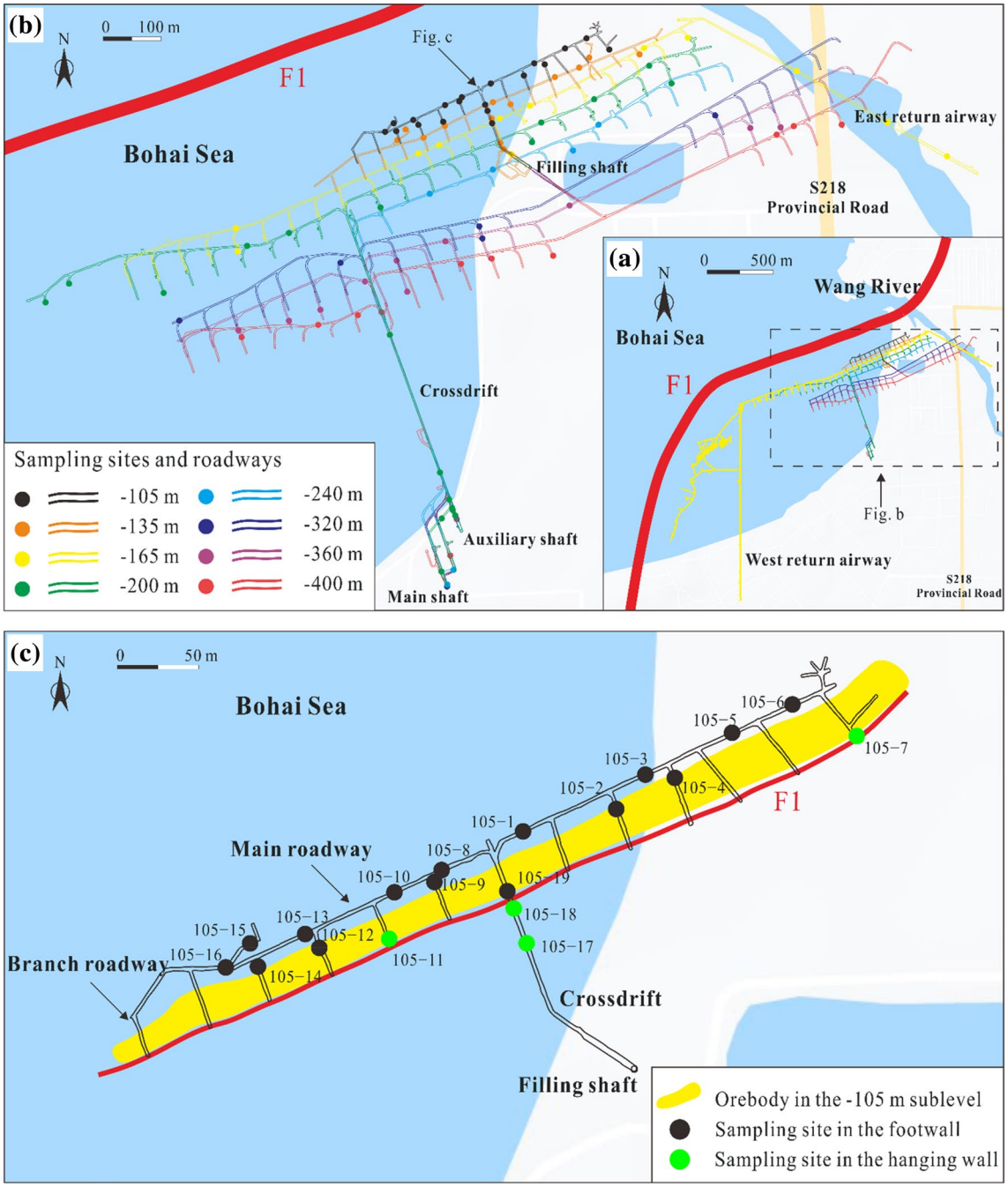

Fig. 2 **a** Insert plan view map showing the location of the underground roadways in the Xinli gold mine. **b** Close-up plan view map showing the location of the sampling sites in the underground roadways. **c** Location of the sampling sites in the − 105 m sublevel in the hanging wall and footwall

In 2006, at the initial stage of mining, 97 water samples were collected in various sublevels (− 105, − 135, − 165, − 200, − 240, − 280, − 320, − 360 and − 400 m sublevels) of the Xinli gold mine. Since then, from 2011 to 2018, the mine water samples were collected regularly in August each year. A total of 245 water samples have been collected, including those from 2006. In addition, two seawater samples, four freshwater samples, and five saline water samples were collected in 2006. Seawater samples were obtained in the Bohai Sea by pumping 1 m below the surface. Freshwater was collected in the upstream portion of the Wang River (see Fig. 1a). Saline water was obtained from the Quaternary aquifer at a depth of 30 m by drilling south of the mining area.

Duplicate water samples were collected in two 600-mL brown polyethylene plastic bottles at each sampling site. The sampling bottles were rinsed with mine seepage water before collection. When the water spilled out of the bottle, the bottle was capped. Finally, the collected water samples were preserved at 5 °C until analysis. The same approach was used for all water samples, including the seawater, groundwater and Wang River water.

Two water samples collected at each sampling site were used for hydrochemical and stable isotope analysis. The water chemical analysis was carried out in the State Key Laboratory of Earthquake Dynamics Institute of Geology, China Earthquake Administration. The major ions (K, Na, Ca, Mg, Cl, SO_4) in the water samples were determined using DIONEX-500 ion chromatograph based on the test method and standards of the People's Republic of China (GB11904-89, GB7477-87, GB7476-87 and GB 11899-89). The stable isotope analysis of the mine water samples was carried out at the laboratory for stable isotope geochemistry, Innovation Academy for Earth Science, CAS using a MT-253 mass spectrometer. The hydrogen-isotope ratio was analyzed using a hydrogen equilibration technique. The oxygen-isotope-ratio was analyzed using a H_2O–CO_2 equilibrium technique. The results were expressed as Vienna Standard Mean Ocean Water (VSMOW) per mil (‰). The analytical precisions of the stable isotopes were 0.2 ‰ for $\delta^{18}O$ and 2 ‰ for δD.

For a more comprehensive analysis of the mixing effects of mine waters in the study area over time, nine years of mine water data from nine sublevels were used for analysis.

Methods for Calculating Mine Water Mixing Ratios

Traditional methods for calculating mine water mixing ratios include the comprehensive analysis of hydrochemistry and isotopes, and PCA (principal component analysis). Hydrochemical and isotopic analysis of collected water samples was used to determine mixing ratios and identify mine water sources in this study and were used in PCA. These methods can do well in the identification of water sources when there is a single type of brine. But if the types of the brine are complex, like in this study area, the traditional methods will not solve the problem clearly and accurately. To address the complexity issue, in addition to using PCA, we applied the hierarchical-multi-index analysis (HMIA) method to identify the mine water sources. In general, the HMIA method has been a breakthrough in identifying mine water sources (Guo et al. 2015; Li et al. 2017; Ma et al. 2015). Both the hydrochemical and isotopic analysis results were used in the HMIA evaluation. The bedrock brines in the study area were preliminarily classified into four types using the hydrochemical method, which were related to its spatial position; thus, according to the spatial feature of the brine, the study area was divided into three levels. On this basis, five pairs of indicators were selected to identify the mine water at each level.

Results

Hydrochemical and Isotopic Analysis and PCA

The results of the hydrochemical testing are shown in Table 1, which presents minimum, maximum, and average values for all mine water samples and average values for the two seawater samples, four freshwater samples, and five saline water samples.

The wide range of concentrations in the mine water samples indicates great differences in characteristics and that the compositions were complex. The average concentrations of the ions and TDS of the mine water samples, which contained some bedrock brines, were higher than those of the seawater, freshwater, and saline water samples, showing the influences of bedrock brines on the area's groundwater. Seawater samples had the maximum average values of the isotope ratios ($\delta^{18}O$ and δD), while the freshwater samples had the minimum average values.

According to the test results and the hydrogeological condition, it could be inferred that the mine water might have had four water sources: seawater, freshwater, saline water, and brine. The compositions of seawater, freshwater, and saline water were relatively stable. However, the brine in the study area had complex compositions, and the types and characteristics of the brine were not obvious because its formation environment, including paleoclimate, paleogeographic environment, and tectonic movement, was complex. Therefore, the different types of brines had to be identified to aid in the identification of mine water sources.

Table 1 Analysis results for all water samples, including isotope ratios (‰), major ions (mg/l), and total dissolved solids (TDS) (mg/l)

	Mine water			Seawater	Freshwater	Saline water
	Minimum	Maximum	Mean			
Sample numbers	241			2	4	5
$\delta^{18}O$	− 7.98	− 1.06	− 3.02	− 0.200	− 7.96	− 2.32
δD	− 60.7	− 5.93	− 27.8	− 5.41	− 56.9	− 24.5
Na	2730	25,300	14,500	8930	192	10,300
Ca	437	7670	2140	387	132	455
Mg	9.70	5030	1810	1120	24.8	1130
Cl	5020	61,200	29,300	16,400	285	18,000
SO_4	456	5280	2830	2350	217	2440
TDS	9400	97,800	51,900	29,700	1120	32,800

Figure 3 shows the results of the hydrochemical analysis (limited to $\delta^{18}O$ and Cl) and PCA. The mine waters are represented by circles and the water end members are represented by triangles in the plot. The water end members are based on the hydrochemical results, as shown in Fig. 3a. Figure 3a shows the hydrochemistry and isotope analysis results, using $\delta^{18}O$ and Cl as conservative indicators (Duan et al. 2019b). However, the high concentration of Cl and other ion characteristics are not reflected in this plot and so the different types of brines in Fig. 3a could not be clearly distinguished using these parameters. Relative to other water end-members, they were all located at the top of the plot and there was no significant distinction between these brines. Another problem was that an actual brine end member that had a relatively low concentration of Cl might be ignored compared to a brine with a high concentration of Cl, such as Brine 4, represented by the red triangle in the plot.

In PCA, the main components (the pc1 and pc2 in Fig. 3b) were obtained by dimension reduction of the original data and were used to represent the original indicators. However, some key characteristics of the indicators might be "neutralized" during the dimension reduction process. Thus, as with the isotopes and hydrochemistry method, the PCA method did not clearly distinguish between different brines (see Fig. 3b). In addition, the different types of mine waters (named Groups 1 and 2 in Figs. 3a, 3b) were not obviously different. The Group 1 water samples were all located in the − 240 m sublevel and below (deep sublevels), while, the Group 2 water samples were all located above − 240 m sublevel (shallow and middle sublevels). And the Group 2 water samples were more like Brine 4 than the Group 1 water samples (see Fig. 3a). However, using different indicator parameters created an obvious difference between the two groups of mine waters, as shown in Fig. 4; in fact, Group 1 and Brine 4 belonged to the same category. Therefore, the traditional methods might ignore the actual brine end member or even select a wrong brine end member when there were different types of brines, and could not clearly show the differences between the mine waters.

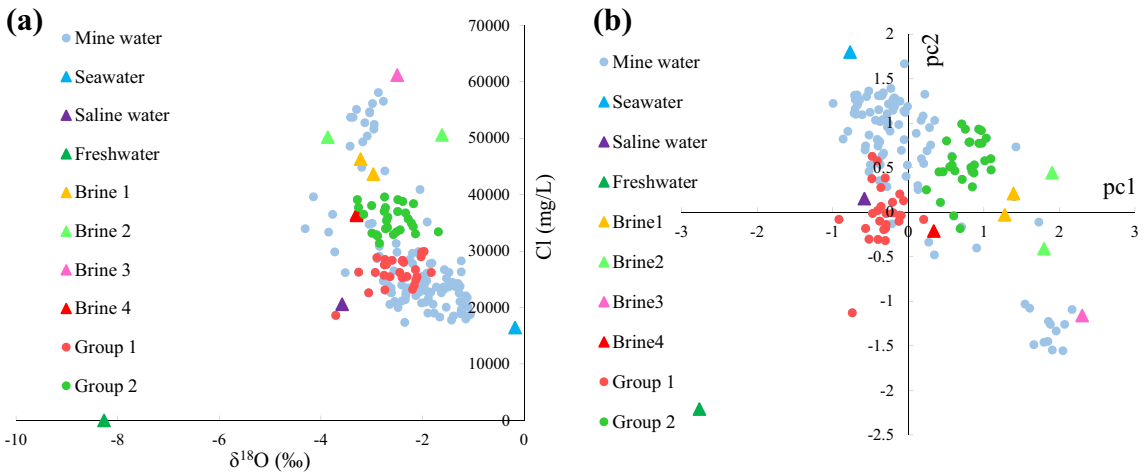

Fig. 3 **a** Relationship between $\delta^{18}O$ and Cl for all water samples. **b** Relationship between pc1 and pc2 for all water samples

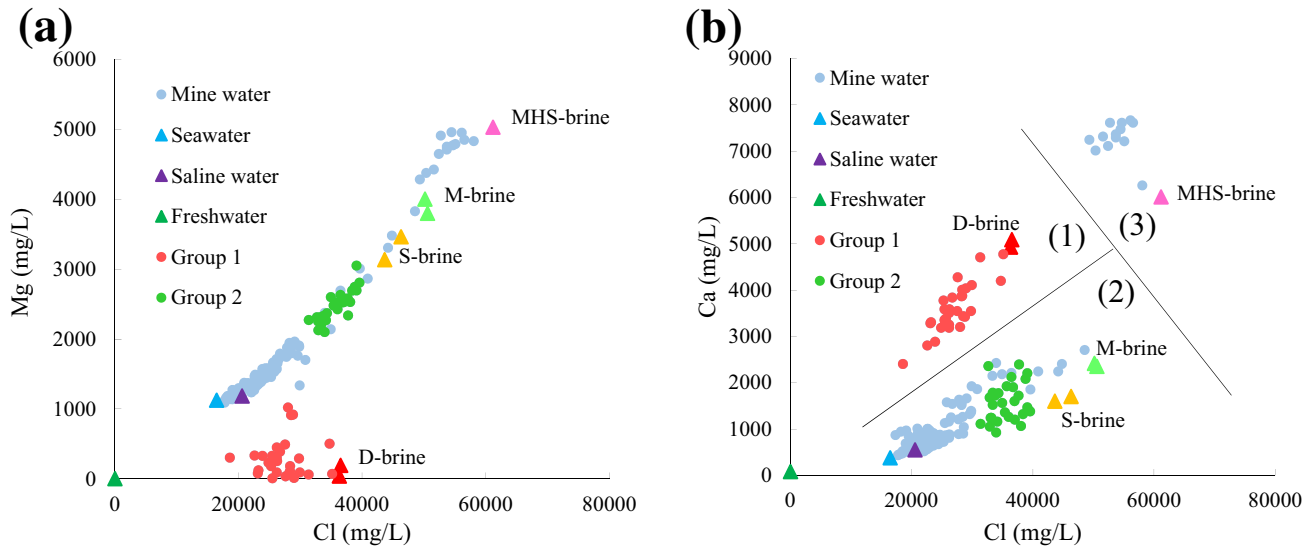

Fig. 4 Correlation of selected major ions in all water samples. **a** Cl vs. Mg. **b** Cl vs. Ca

Considering the limitation of using the parameters in Fig. 3, the correlation between Cl and other ions (Ca and Mg) was evaluated (Fig. 4). In the plot, circles and triangles were used to represent mine waters and potential water sources, respectively. In Fig. 4a, the Mg concentration in most water samples showed an obvious positive correlation with Cl, but some of the water samples (named group1 and marked red on the plot) deviated from the correlation. The characteristic of Group 1 water samples was that they had a low Mg concentration (Fig. 4a) and a relatively high Ca concentration (Fig. 4b). These water samples were all located in the − 240 m sublevel and below (deep sublevels). This indicated that in the deep sublevels, brines with a low Mg concentration and high Ca concentration were mixing with the mine water. The 240-2 and 320-7 water samples were representative of this brine, and because of the spatial position of this brine it was called D-brine (deep brine). In addition to the D-brine, there were three possible brine end members (Fig. 4), which were named according to their spatial position and features. The 105-16 and 135-9 water samples were called S-brine (shallow brine) and had the highest concentrations of SO_4 of all the water samples. The 165-11 and 200-15 water samples were called M-brine (middle brine). The M-brine was similar to the S-brine, but had higher TDS and a lower SO_4^{2-} concentration than the S-brine. The 165-10 water sample was called MHS-brine (middle high-salinity brine) because it had the highest TDS of all the water samples. In Fig. 4a, these three types of brines (S, M, MHS) showed a linear relationship between Mg and Cl. In Fig. 4b, all of the water samples could be classified into three categories: the deep mine waters which were mainly affected by the D-brine (red symbols in Fig. 4b); the water samples without a consistent linear relationship between Ca and Cl (some samples fell on the mixing line defined by the S-brine, seawater, and saline water, while others fell above that mixing line and were potentially influenced by the M-brine); and the MHS-brine, which included samples 165-6, -7, -8, -9, and -10, which were located in the western return airway in the hanging wall and far from the other sites (see Fig. 2a).

In summary, bedrock brines with different chemical characteristics were located at different depths. Four types of brines were preliminarily identified: S-brine, M-brine, MHS-brine, and D-brine. But the relationships between them and the other water samples were still unclear. Therefore, the HMIA method was proposed for further study.

Hierarchical Multi-index Analysis

The study area was divided into three levels vertically according to the spatial position of the different brines: shallow sublevels (− 105 and − 135 m sublevels), middle sublevels (− 165 and − 200 m sublevels), and deep sublevels (− 240 m sublevels and below). The HMIA was carried out at each level separately, which simplified and clarified the water source identification process. Four pairs of indicators that could reflect the characteristics of the water end members were selected from five pairs of indicators (Cl–$\delta^{18}O$, Cl–Ca, Cl–Mg, Cl–SO_4, Cl–Na). Table 2 shows the indicators selected for analysis at each level.

Specifically, the mine water samples in the − 165 m sublevel and below from 2006 were not analyzed because most of these samples were affected by water inflow ("filling water") during the initial stages of mining. Filling water refers to the water used to fill the gob and is imported from outside sources to the mine.

Table 2 Analysis indicators used for each level

Level	Sublevels	Analysis indicators
Shallow	− 105 m and − 135 m	Cl–δ^{18}O, Cl–Mg, Cl–Ca, Cl–SO_4
Middle	− 165 m and − 200 m	Cl–δ^{18}O, Cl–Mg, Cl–Ca, Cl–Na
Deep	− 240 m and below	Cl–δ^{18}O, Cl–Mg, Cl–Ca, Cl–Na

Water Source Identification in the Different Sublevels

The Shallow Sublevel

In Fig. 5, triangles and circles were used to represent potential water sources and mine waters, respectively. The "Mixing boundary" and the "Mixing line" refer to the connection between each end member. When the end members are not colinear, it is a mixing boundary (Fig. 5a); if colinear, it is a mixing line (Figs. 5b–d). The mine waters included two types: one (dark blue circles in Fig. 5) was mine water samples from 2006 and the other (light blue circles in Fig. 5) was mine water samples collected after 2006. The distribution of the water chemistry data from the shallow sublevels was relatively concentrated (Fig. 5), which indicated that the composition of these mine waters was relatively simple. In Fig. 5a, all of the mine waters were located on and above the lower boundary of the mixing line described by seawater and saline water and far from the freshwater. It showed that seawater and saline water were two of the end members of the mine water in terms of δ^{18}O values, and freshwater made little contribution to the mixing of the mine water. Because the shallow sublevels were entirely under the sea, the recharge of freshwater was limited. The four types of brines were another potential end member in terms of Cl concentrations because they were all in the upper mixing boundary. Figure 5b shows that the D-brine was not an end-member of shallow sublevel mine water because all of the water samples showed a linear relationship and had no trend of deflection to the D-brine. Similarly, the MHS-brine was not an end member of the shallow sublevel mine water

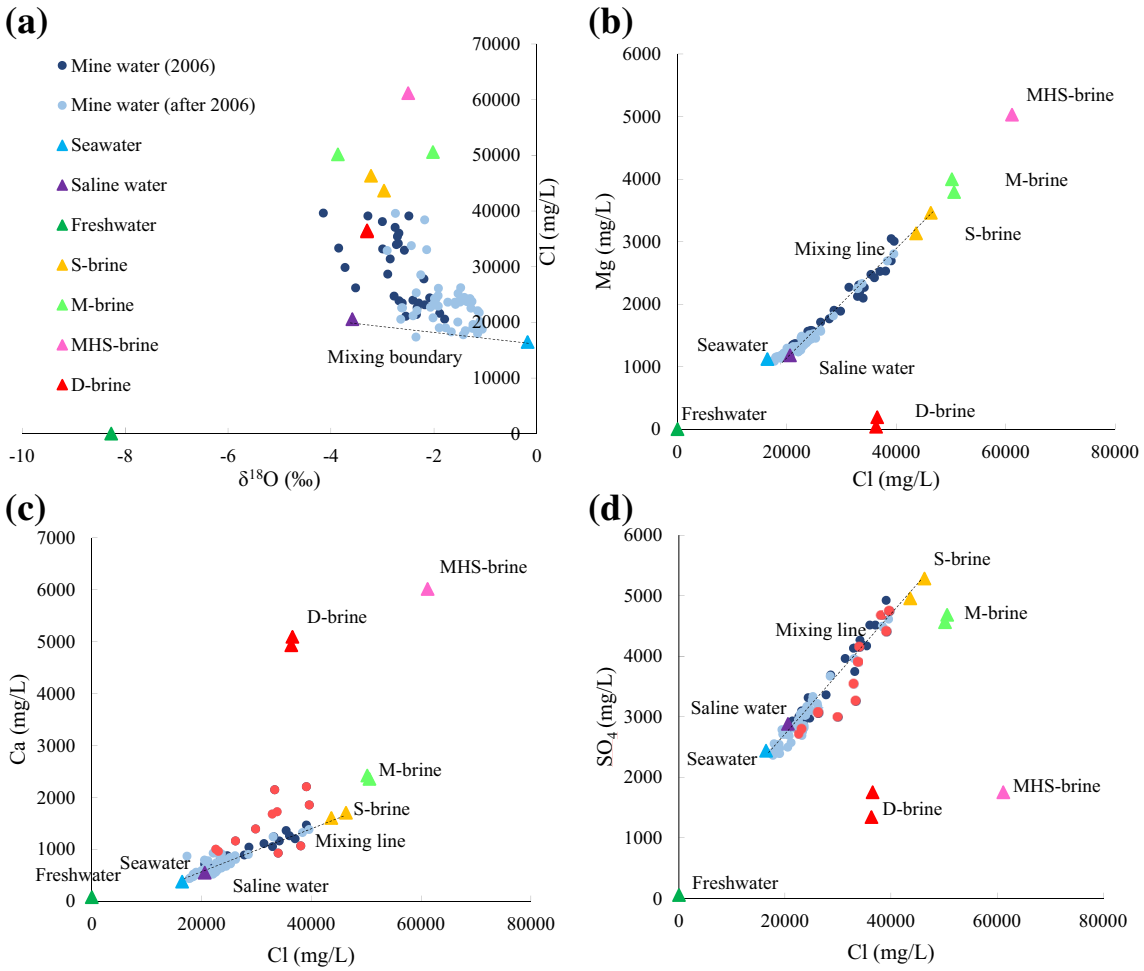

Fig. 5 Correlation of indicators in water samples from the shallow sublevels. **a** Cl vs. δ^{18}O. **b** Cl vs. Mg. **c** Cl vs. Ca. **d** Cl vs. SO_4

(Fig. 5d). Figure 5b–d show that most of the shallow sublevel mine waters fell on the mixing line described of seawater, saline water, and S-brine, while the M-brine deviated from this linear relationship. In addition, some mine waters (marked red in Fig. 5c) deviated from the linear relationship. The common feature of these mine waters was that they were located in the branch roadways through the orebody near the hanging wall (see Fig. 1c), while the other mine waters were located in the main roadway, in the footwall. The results suggest that the mine waters might be affected by local water in the hanging wall. The mixed mode (sources) of the mine water in the shallow sublevels was seawater-saline water-shallow brine. In addition, compared with the mine waters from the initial stage of mining, the mine waters after 2006 had an obvious evolutional trend toward seawater over time. Overall, the mine waters collected after 2006 had chemical characteristics closer to seawater in all Fig. 5 plots, indicating that the movement and evolution of groundwater in this area were affected by mining.

The Middle Sublevels

The high salinity brines represented by 165-10 (the MHS-brine) are marked red in Fig. 6. In Fig. 6a, both M-brine and MHS-brine could be the brine end members of the mine water in terms of Cl concentrations. These high salinity brines (marked with red circles in Fig. 6) showed a different linear relationship with other mine waters in Fig. 6d. Also, in Fig. 6c, the distance between these brines and other water samples showed that they had a weak hydraulic connection with the other mine waters, suggesting that the MHS-brine was not a brine end member of the mine water at this sublevel and its influence was limited. Similarly, the D-brine was not a brine end member, as shown in Fig. 6b and c). In Fig. 6b–d, the mine waters fell around the mixing line described by seawater, saline water, and M-brine. In Fig. 6a, the mine waters fell in the mixing boundaries composed by the above three brine end members. As with the shallow sublevels, the middle sublevels were almost all located under the seafloor and the effect of freshwater could be ignored.

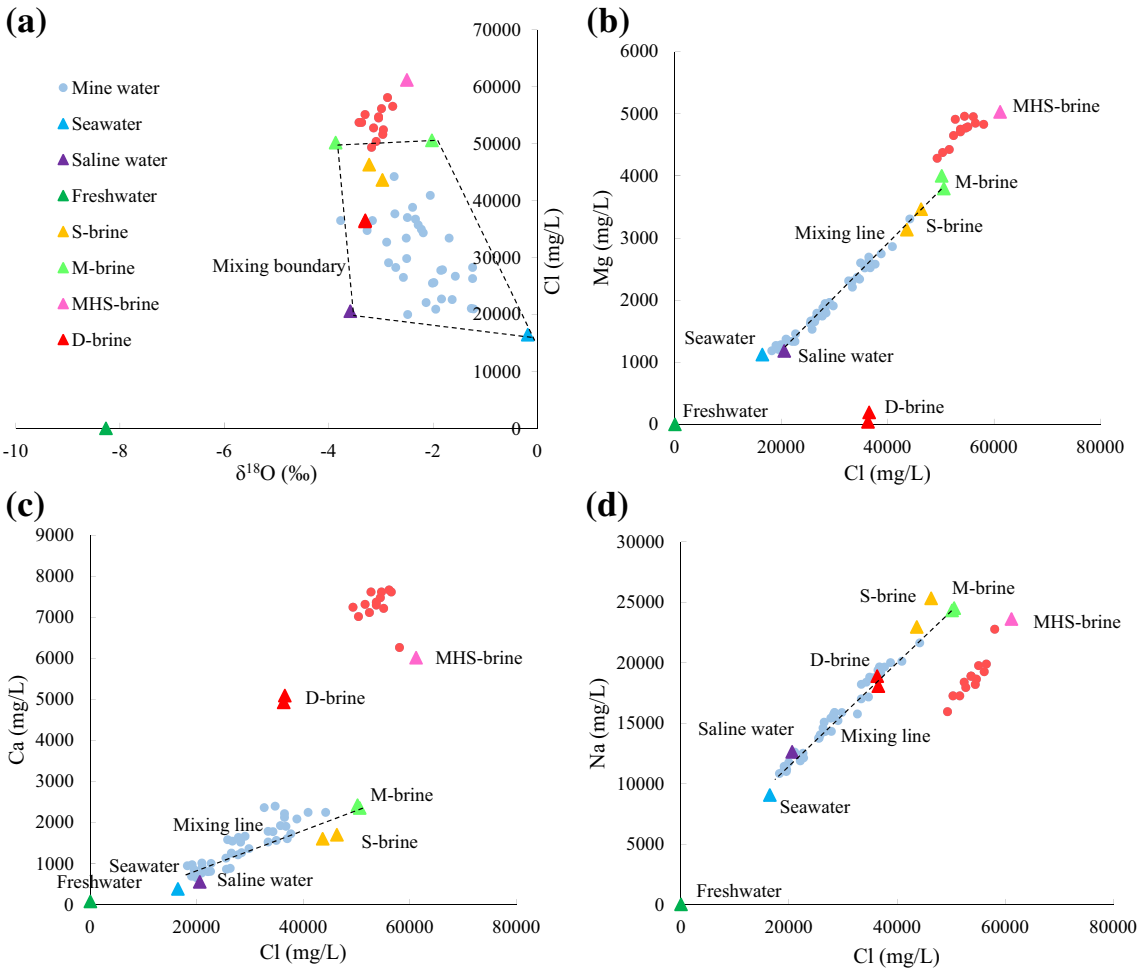

Fig. 6 Correlation of indicators in water samples from the middle sublevels. **a** Cl vs. $\delta^{18}O$. **b** Cl vs. Mg. **c** Cl vs. Ca. **d** Cl vs. Na

In summary, in the middle sublevels, the mixed mode of the mine water was seawater-saline water-middle brine.

The Deep Sublevels

Compared with the mine waters in the middle sublevels (Fig. 6a), most of the mine waters in the deep sublevels showed a centralized data distribution (Fig. 7a) and were mainly distributed near the D-brine (Fig. 7a and d), indicating that the D-brine played a dominant role in the mixing of mine water in the deep sublevels and that seawater and saline water played a relatively small role. Some of the water samples (marked red in Fig. 7b, c) belonged to the mixed mode of the middle sublevels and a transition mode that was between the above two mixed modes. Because some of the mine waters looked like the mixed mode of both the middle and deep sublevels, they were called transition mode; the dashed line shows the trend of this transition. The results also indicated that there was a hydraulic connection between the middle and deep sublevels. In addition, freshwater influenced the mine water because the mixing relationship of the mine water deviated to the freshwater (Fig. 7b and c). But the effect of freshwater was relatively small, as shown by the distance between the fresh and mine water (Fig. 7b–d). The position of the deep sublevels could explain the effect of the freshwater. Most of the deep sublevels were located under land and could be recharged by freshwater. In conclusion, the mixed mode of the mine water in the deep sublevels was mainly: seawater-saline water-deep brine.

Discussion

Classification of Bedrock Brines

Although important discoveries were revealed by previous studies, there were also limitations. First, on the time and

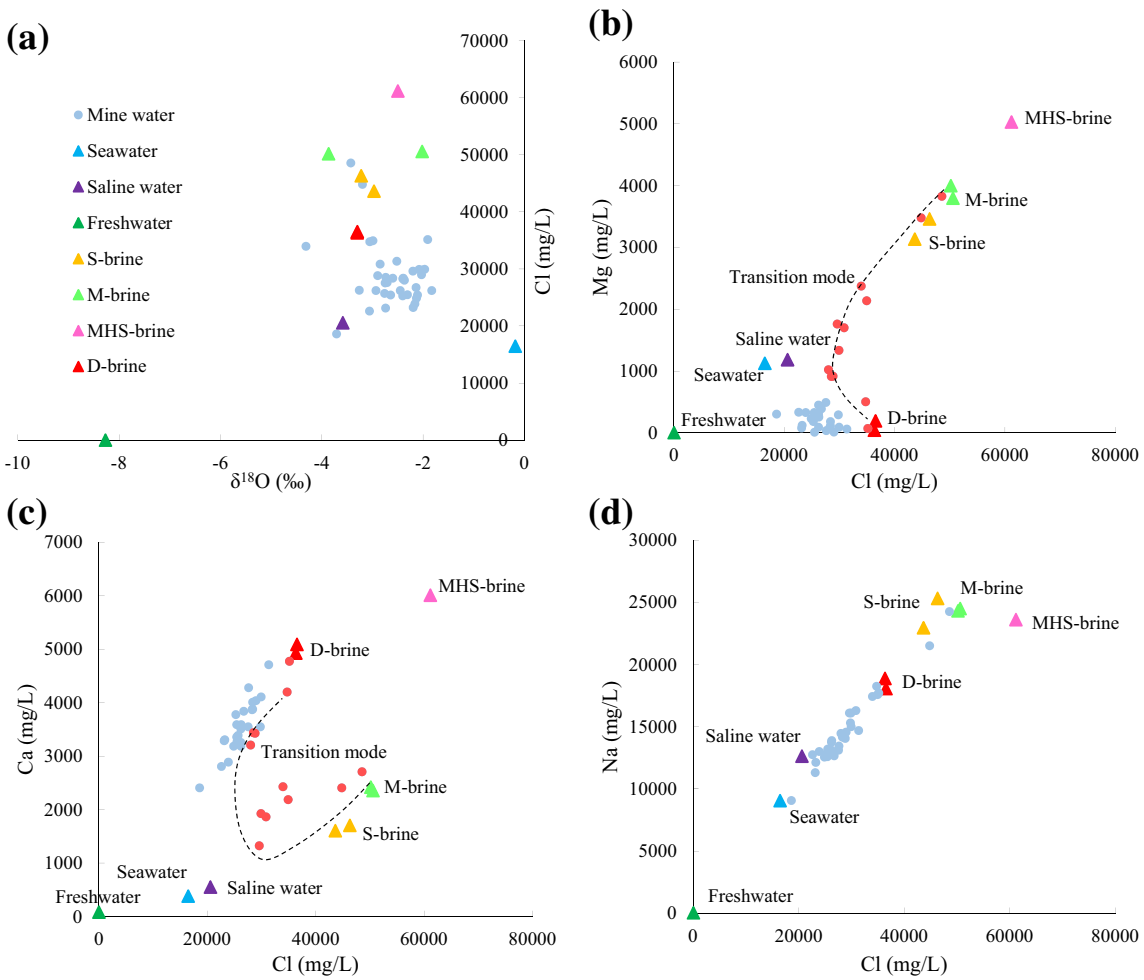

Fig. 7 Correlation of indicators in water samples from the deep sublevels. **a** Cl vs. $\delta^{18}O$. **b** Cl vs. Mg. **c** Cl vs. Ca. **d** Cl vs. Na

regional scale, most of the previous studies only considered the mine waters of the shallow sublevels at the initial stage of mining. Second, the methods used in the previous studies were not suitable for sites with complex conditions.

Compared to the previous studies, this study identified the various types of bedrock brines in the Xinli mining area. And the spatial location of the different brines is the basis and key to identifying the mine water sources in the study area. The geographical location of the study area can explain the spatial feature of the brine. Since the late Pleistocene, there have been three large-scale marine transgressions in the area due to climate change and sea level eustacy during the ice age and interglacial stage. This led to creation of underground brines in the area. Many researchers have studied the origin of brines in this area (Chang et al. 2018; Li and Meng 2014; Ma et al. 2007; Wang et al. 2003). They believe that there was a large marine transgression period before the deposition of the Quaternary deposits in this area, and this resulted in a large amount of seawater entering fissures in the bedrock. Subsequent regression led to intensive evaporation and gradual concentration of seawater in the bedrock. The deposition of the Quaternary sediment sealed the concentrated ancient seawater in the bedrock fissures. Isotope and hydrochemical analysis show that the brines originated from ancient seawater and were similar to modern seawater but with higher ion concentrations than modern seawater. Li et al. (2012) used characteristic chemical composition SO_4 (in meq/L)/Cl (in meq/L) (meq/L or millimoles equivalent per liter equals mg/L multiplied by its atomicity and divided by its molecular weight) to analyze the reason for the formation of the bedrock brine in the study area. The principle of this method is that SO_4 and Cl are the primary anions in seawater and the SO_4(meq/L)/Cl(meq/L) ratio of seawater is constant between 0.10 and 0.15. However, if the chemical environment gradually changes from oxidizing to reducing conditions, that is, if the area where the water is stored is closed to the atmosphere for a long time, desulfurization will occur. Therefore, the SO_4(meq/L)/Cl(meq/L) ratio of concentrated and ancient seawater exposed to reducing conditions would be less than that of seawater in an open system, and the more reducing the conditions, the lower the ratio. Table 3 shows the SO_4(meq/L)/Cl(meq/L) ratios of different water samples. The ratios in the three kinds of bedrock brines are all less than that of seawater and the values decrease with greater burial depth. In addition, the mineralogy of the depositional environment can also affect the chemistry of the brine. The samples from different stages have diverse mineral assemblages and geochemical characteristics due to the processes of alteration and mineralization (Yang et al. 2015, 2018). Zhao et al. (2015) found the carbonation (ore) samples to have a high CaO content in the − 240 m sublevel. This can explain why the D-brine had high Ca and low Mg concentrations. In summary, the paleoclimate, paleogeographic environment, tectonic movement, and metallogenic environment of this area led to the spatial and chemical features of the bedrock brine.

Mixing Ratio Calculation and Deviation Analysis

According to the water source identification results, the mine water in the shallow sublevels is a mixture of seawater, saline water, and shallow brine (105-16 or 135-9). Therefore, a ternary diagram can be used to calculate the mixing ratio of these end members in mine water, and the reliability and accuracy of the new method can be evaluated by comparing the deviation analysis with the previous research results (Liu et al. 2007). The deviation can be calculated using the following equation for a given parameter:

$$D = \frac{|C_c - C_m|}{C_m} \times 100\%$$

where C_c is the computed concentration of indicators and C_m is the measured concentration. The computed concentrations can be obtained through back calculation by using the end-members concentrations and the result of the mixing ratios.

Ma et al. (2015) selected a high-salinity brine (from a saltern near the study area) as the brine end member, created a ternary diagram, and determined the mixing ratio of the end members in mine water. However, the brine end member in their study only had isotopic ratios and TDS concentrations, and it is not possible to calculate the deviation of other indicators. Therefore, we selected a brine sample with a similar composition (the isotope ratios of $\delta^{18}O$ and δD, and the TDS concentration) and high salinity for analysis, obtained the same mixing ratio results as the previous study, and calculated the deviation values for each indicator. In our study, water sample 105-16 (shallow brine) was selected as the brine end member to plot on a ternary diagram, and the mixing ratios and deviation values were calculated using the same method used in previous studies.

Table 3 SO_4 (meq/L)/Cl (meq/L) of different water samples

	Seawater	Shallow brine		Middle brine		Deep brine	
		105-16	135-9	165-11	200-15	240-2	320-7
SO_4 (meq/L)/Cl (meq/L)	0.11	0.08	0.08	0.07	0.07	0.03	0.04

Figure 8a shows the average proportion of seawater in mine water over time for the two studies and Table 4 shows that the deviation values for the mixing ratio in this study have been greatly improved compared with previous studies, thus demonstrating the value of using HMIA and water source identification.

The proportion of seawater calculated by the previous study was relatively high, especially in the initial stage of mining (2006) when the average proportion of seawater in the mine water reached 39%. The proportion of seawater in the mine water at that time using results from this study was 22%, which was more in line with the actual situation (the proportion of seawater should be relatively low at the beginning of exploitation). In addition, the proportion of seawater increased every year, but the rate gradually slowed down. The three water samples with the highest proportion of seawater were averaged for the − 105 m and − 135 m sublevels. Because the number of water samples in these two sublevels (− 105 m and − 135 m sublevels) was different (some of the water samples had a particularly low proportion of seawater), three samples were selected for comparison. Figure 8b shows the results. The proportion of seawater in the − 105 m sublevel was higher than that in the − 135 m sublevel, but the difference decreased over time (see Fig. 8b). The results demonstrate that seawater first affected the upper sublevel, suggesting that seawater mainly infiltrated by vertical recharge from Laizhou Bay. As mining progressed, blasting likely increased the density of fractures between the two sublevels, forming a hydraulic connection. Figure 8b also shows that the proportion of seawater increased over time, but the rate slowed down or even decreased.

Interpolation of the seawater proportion for all mine water samples from 2006 in the − 105 m sublevel is shown in Fig. 9. The water samples collected from the footwall had a high proportion of seawater; for example, water samples 105-1, -2, -9, and -10 contained nearly 50% seawater. Water samples 105-7, -17, -18, and -19 on the hanging wall all had a low proportion of seawater. In addition, water samples 105-14, -15, and -16 on the east side of the sublevel also had a relatively low proportion of seawater. This shows that the water-conducting fractures are mainly in the footwall where the mining activity was concentrated and extended from the middle to both sides of the cross drift (see Fig. 2c) as the mining project advanced.

For a more comprehensive analysis of the mine seepage water, flow data from four continuously monitored mine water sampling sites are shown in Fig. 10. For most water sites (105-1, 105-14, and 135-12) the flow increased gradually from the beginning of mining, but then it would stabilize, and finally, decrease. The same pattern can be seen in the changes of Cl concentration at each water site (see Fig. 11). This is likely because the fractures in the initial stage of mining formed a hydraulic connection to the bedrock brine, which increased the flow rate, but the inflow of bedrock brine decreased substantially in 2012.

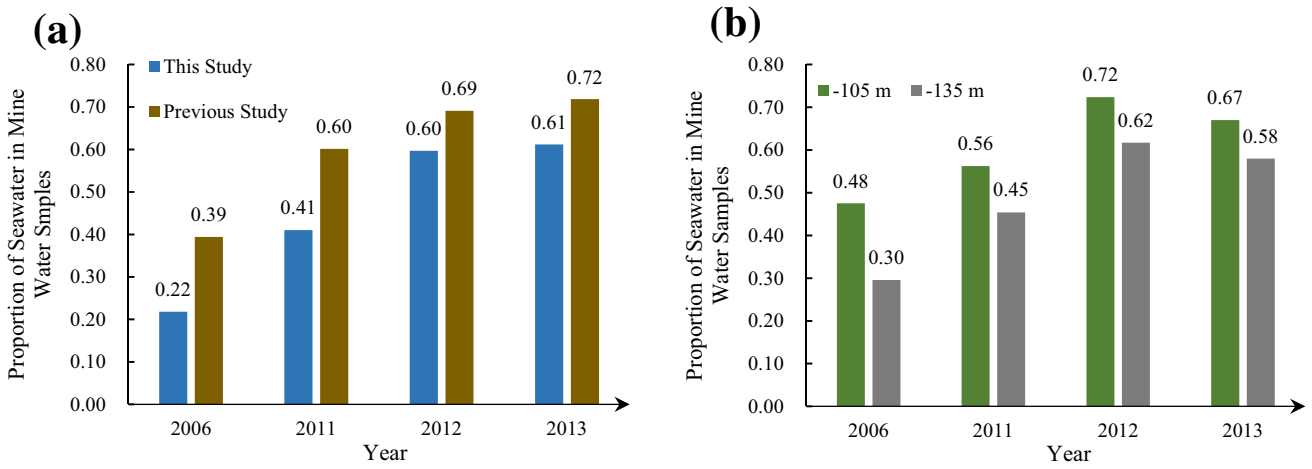

Fig. 8 Average proportion of seawater in mine water over time. **a** Mixing ratios for the two studies in the shallow sublevels. **b** Mixing ratios for samples with the highest proportion of seawater from the − 105 m and − 135 m sublevels (this study)

Table 4 Deviation values[1] of δD and all ions in two studies

	δD	Cl	SO_4	Na	Ca	Mg
Ma et al. (2015)	0.39	0.07	0.44	0.19	0.21	0.32
This study	0.40	0.02	0.05	0.03	0.14	0.05

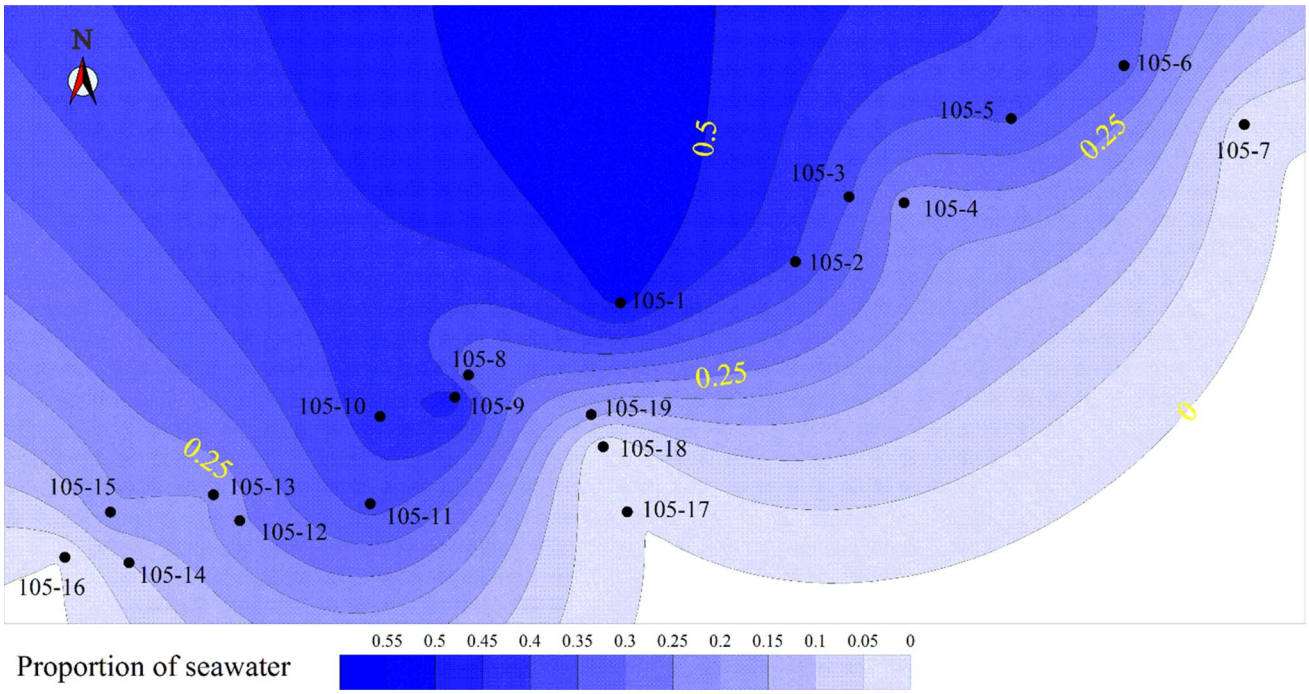

Fig. 9 Plan view of the − 105 m sublevel showing the spatial distribution of seawater proportion for all water samples in − 105 m sublevel in 2006

Overall, classifying different types of bedrock brine is very important when identifying water sources in an area known to have underground brines. Our study classified different types of bedrock brines based on their chemical and stratigraphic features to help identify mine water sources. In addition, the validity of the bedrock brine classification and water source identification was evaluated using water quality characteristics and mixing ratio deviation, respectively. On this basis, the mixing ratio of different sources of mine water in the shallow sublevels was calculated, especially the proportion of seawater in the upper sublevel (− 105 m). The mixing ratio of mine waters in the middle and deep sublevels was not calculated because mine water in these sublevels may be influenced by the upper layers, which means that the ternary diagram is not suitable for calculating the mixing ratio. We are currently investigating other approaches for determining the mixing ratio of mine water in the middle and deep sublevels to provide information to improve safe production in the mine.

Conclusion

This study identified different types of bedrock brines in the Xinli gold mine. On this basis, the HMIA method was used to identify mine water sources and the mixing ratio of mine water in the shallow sublevels was calculated using a ternary diagram. This method could be applied to water source identification of nearby mines with similar geological conditions. The specific conclusions are:

(1) The bedrock brine in the study area was classified into four brine types: shallow, middle, middle high-salinity, and deep. The bedrock brine classification was evaluated using brine genesis analysis and mixing ratio deviation.
(2) The mixed modes in the shallow sublevels, middle sublevels, and deep sublevels were seawater-saline water-shallow brine, seawater-saline water-middle brine, and seawater-saline water-deep brine, respectively. Also, the mine waters in the middle sublevels also affected the deep sublevels.

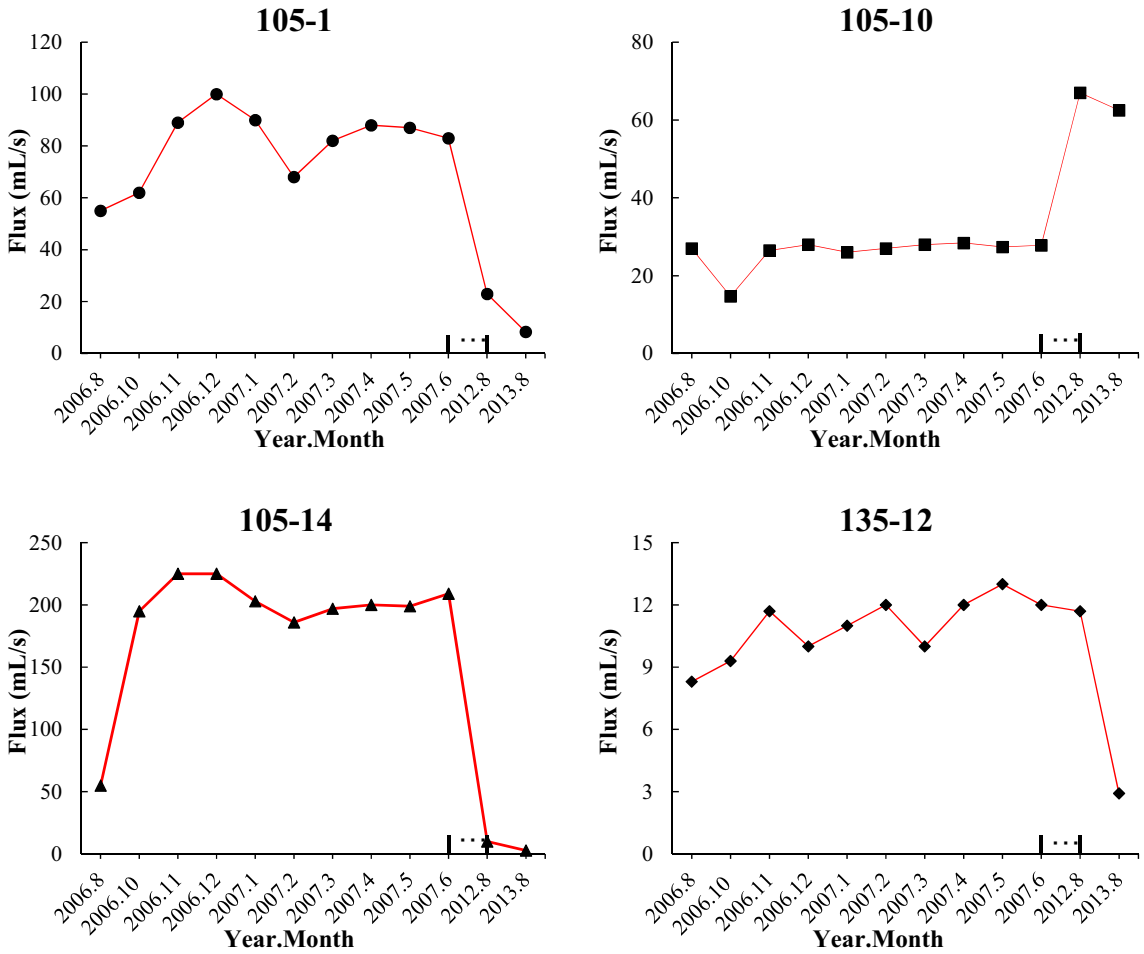

Fig. 10 The flow rate (mL/s) of four mine water sampling sites over time from August 2006 to August 2013

(3) In 2006, 2011, 2012, and 2013, the average proportion of seawater in mine water was 0.22, 0.41, 0.60, and 0.61, respectively. The proportion increased, but the rate of increase slowed down over time.

(4) Seawater had a great influence on the shallow and middle sublevels, especially in the shallow sublevels. In the shallow sublevels, the proportion of seawater in the − 105 m sublevel was higher than that in the − 135 m sublevel, but the difference between the two levels decreased over time, suggesting that seawater primarily infiltrated via vertical recharge.

(5) The mine water sampling sites in the footwall and in the middle of the − 105 m sublevel were nearly 50% seawater, while the sites on the hanging wall had relatively low seawater proportions. This suggest that the water-conducting fractures were mainly in the footwall. Monitoring of water inflow in the middle of the lower sublevel should be increased and protective measures to improve mine and worker safety should be taken.

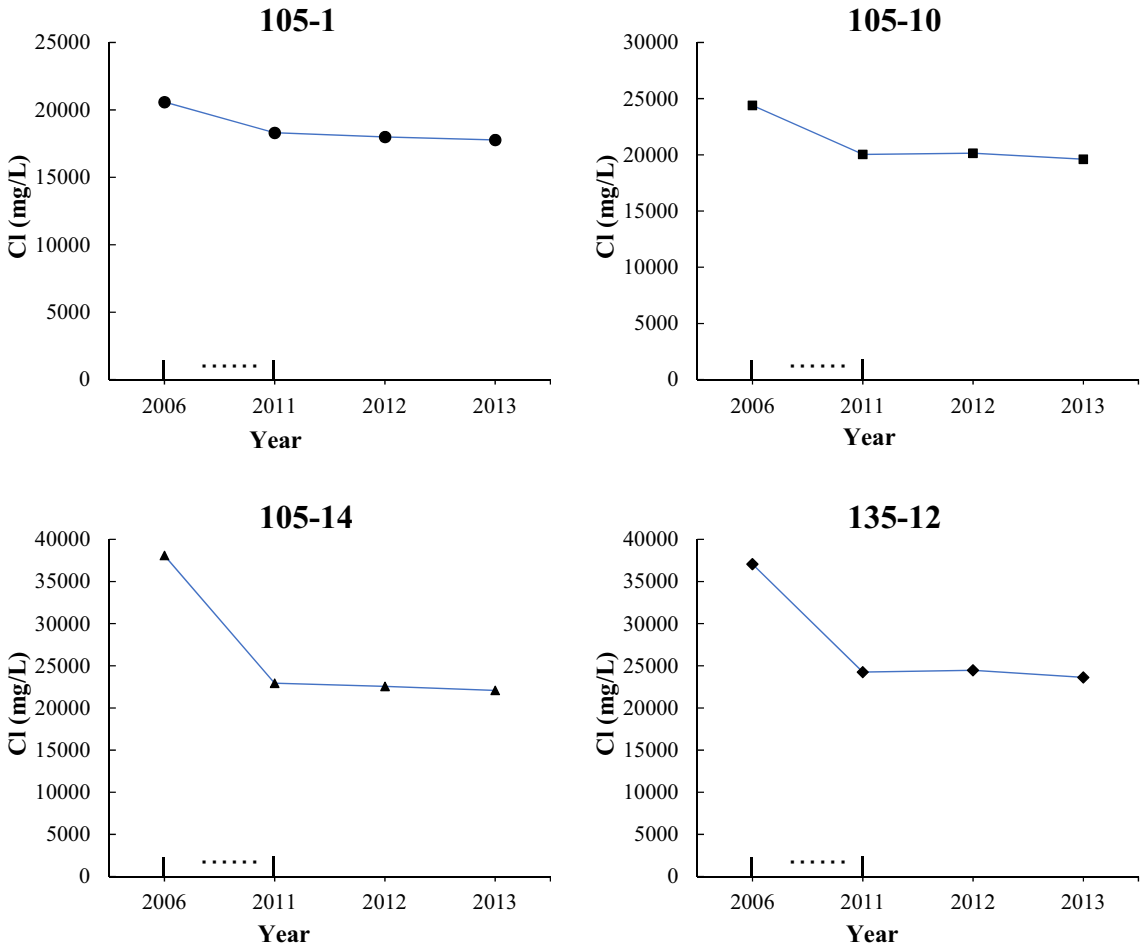

Fig. 11 The concentration of Cl (mg/L) of four mine water sampling sites over time from 2006 to 2013

Acknowledgements This research was supported by the National Natural Science Foundation of China (Grants 41831293 and 41907174). Grateful appreciation is expressed for this financial support.

References

Chang Y, Hu B, Xu Z, Li X, Tong J, Chen L, Zhang H (2018) Numerical simulation of seawater intrusion to coastal aquifers and brine water/freshwater interaction in south coast of Laizhou Bay, China. J Contam Hydrol 215:1–10

Chen Y, Zhao G, Wang S, Wu H, Wang S (2019) A case study on the height of a water-flow fracture zone above undersea mining: Sanshandao Gold Mine, China. Environ Earth Sci. https://doi.org/10.1007/s12665-019-8121-7

Chung J (1996) Deep-ocean mining: technologies for manganese nodules and crusts. Int J Offshore Polar Eng 6:1–11

Dong D, Chen Z, Lin G, Li X, Zhang R, Ji Y (2019) Combining the Fisher feature extraction and support vector machine methods to identify the water inrush source: a case study of the Wuhai mining area. Mine Water Environ 38:855–862

Dong S, Zhang W, Zhou W, Chai R, Wang H, Zhao C, Dong X, Wang Q (2021) Discussion on some topical issues of water prevention and control in coal mines. Mine Water Environ. https://doi.org/10.1007/s10230-021-00773-3

Duan X, Ma F, Zhao H, Guo J, Gu H, Lu R, Liu G (2019a) Determining mine water sources and mixing ratios affected by mining in a coastal gold mine, in China. Environ Earth Sci 78:299

Duan X, Ma F, Guo J, Zhao H, Gu H, Liu S, Sun Q (2019b) Source identification and quantification of seepage water in a coastal mine, in China. Water 11:1862

Fan Y, Chen Y, He Q, Li W, Wang Y (2016) Isotopic characterization of river waters and water source identification in an inland river, central Asia. Water 8:286

Gao M, Zheng Y, Liu S, Wang S, Kong X, Zhao J, Guo F (2015) Palaeogeographic condition for origin of underground brine in southern coast of Laizhou Bay, Bohai Sea. Geol Rev 61:393–400

Gu H, Ma F, Guo J, Li K, Lu R (2017) Hydrochemistry, multidimensional statistics, and rock mechanics investigations for Sanshandao Gold Mine, China. Arab J Geosci 10(3):62

Gu H, Ma F, Guo J, Zhao H, Lu R, Liu G (2018a) A spatial mixing model to assess groundwater dynamics affected by mining in a coastal fractured aquifer, China. Mine Water Environ 37:405–420

Gu H, Ma F, Guo J, Li K, Lu R (2018b) Assessment of water sources and mixing of groundwater in a coastal mine: the Sanshandao Gold Mine, China. Mine Water Environ 37:351–365

Güler C, Thyne G (2004) Delineation of hydrochemical facies distribution in a regional groundwater system by means of fuzzy c-means clustering. Water Resour Res 40(12):W12503

Güler C, Kurt M, Alpaslan M, Akbulut C (2012) Assessment of the impact of anthropogenic activities on the groundwater hydrology and chemistry in Tarsus coastal plain (Mersin, SE Turkey) using fuzzy clustering, multivariate statistics and GIS techniques. J Hydrol 414:435–451

Guo J, Zhao H, Ma F, Li K, Zhao C (2015) Investigating the permeability of fractured rock masses and the origin of water in a mine tunnel in Shandong province, China. Water Sci Technol 72:2006–2017

Jiang C, An Y, Zheng L, Huang W (2021) Water source discrimination in a multiaquifer mine using a comprehensive stepwise discriminant method. Mine Water Environ. https://doi.org/10.1007/s10230-020-00742-2

Laaksoharju M, Skårman C, Skårman E (1999) Multivariate mixing and mass balance (M3) calculations, a new tool for decoding hydrogeochemical information. Appl Geochem 14:861–871

Li P (2018) Mine water problems and solutions in China. Mine Water Environ 37:217–221

Li S, Meng Y (2014) Distribution, origin and development status of underground brine resource along the coast of Laizhou Bay, Shandong Province. Acta Geol Sin-Engl 88(S1):222

Li X, Li D, Liu Z, Zhao G, Wang W (2013) Determination of the minimum thickness of crown pillar for safe exploitation of a subsea gold mine based on numerical modelling. J Rock Mech Min Sci 57:42–56

Li G, Wang X, Meng Z, Zhao H (2014) Seawater inrush assessment based on hydrochemical analysis enhanced by hierarchy clustering in an undersea goldmine pit, China. Environ Earth Sci 71:4977–4987

Li G, Ma F, Meng Z (2012) Analysis of connectivity between undersea metal mine and overlying seawater in Xinli mine area. J Central South University (science and Technology) 43(10):3938–3945 (**In Chinese**)

Li K, Ma F, Zhang H, Li W, Lv Y (2017) Identification and evolution of water source from seabed gold mines. J Eng Geol 01:180–189 (**In Chinese**)

Li W, Liu Y, Qiao W, Zhao C, Yang D, Guo Q (2018) An improved vulnerability assessment model for floor water bursting from a confined aquifer based on the water inrush coefficient method. Mine Water Environ 37:196–204

Li P, Wu J, Qian H (2016) Preliminary assessment of hydraulic connectivity between river water and shallow groundwater and estimation of their transfer rate during dry season in the Shidi River, China. Environ Earth Sci 75:99

Liu Z, Dang W, He X (2012) Undersea safety mining of the large gold deposit in Xinli District of Sanshandao gold mine. Int J Min Met Mater 19:574–583

Liu Z, Luo T, Li X, Li X, Huai Z, Wang S (2018) Construction of reasonable pillar group for undersea mining in metal mine. T Nonferr Metal Soc 28(4):757–765

Liu G, Ma F, Liu G, Zhao H, Guo J, Cao J (2019) Application of multivariate statistical analysis to identify water sources in a coastal gold mine, Shandong, China. Sustainability 11:3345

Liu G, Ma F, Liu G, Guo J, Duan X, Gu H (2020) Quantification of water sources in a coastal gold mine through end-member mixing analysis combining multivariate statistical methods. Water 12:580

Liu C, Peng B, Qin J (2007) Geological analysis and numerical modeling of mine discharges for the Sanshandao gold mine in Shandong, China: 1. geological analysis. Mine Water Environ 26(3):160–165

Ma F, Yang Y, Yuan R, Cai Z, Pan S (2007) Study of shallow groundwater quality evolution under saline intrusion with environmental isotopes and geochemistry. Environ Geol 51:1009–1017

Ma F, Zhao H, Guo J (2015) Investigating the characteristics of mine water in a subsea mine using groundwater geochemistry and stable isotopes. Environ Earth Sci 74:6703–6715

Mauryaa P, Kumaria R, Mukherjeeb S (2019) Hydrochemistry in integration with stable isotopes ($\delta^{18}O$ and δD) to assess seawater intrusion in coastal aquifers of Kachchh district, Gujarat, India. J Geochem Explor 196:42–56

Peng K, Li X, Wang Z (2015) Hydrochemical characteristics of groundwater movement and evolution in the Xinli deposit of the Sanshandao gold mine using FCM and PCA methods. Environ Earth Sci 73:7873–7888

Peng K, Li X, Wan C, Peng S, Zhao G (2011) Safe mining technology of undersea metal mine. T Nonferr Metal Soc 22(3):740–746

Rona P (2003) Resources of the sea floor. Science 299:673–674

Su Q, Yu H, Peng C, Xu X (2011) Hydrochemical characteristics of underground brine in littoral plain south of Laizhou Bay. Adv Mar Sci 29:163–169

Sui W, Xu Z (2013) Risk assessment for coal mining under sea area. New Front Eng Geol Environ 9:199–202

Wang Z, Meng G, Wang S (2003) Geochemistry modeling of quaternary subsurface brines in south coast of the Laizhou Bay, the Bohai Sea—taking brines from core-Aoli501 in Changyi area as an example. Mar Geol Q Geol 01:49–53 (**In Chinese**)

Wu Q, Guo X, Shen J, Xu S, Liu S, Zeng Y (2017) Risk assessment of water inrush from aquifers underlying the Gushuyuan coal mine, China. Mine Water Environ 36:96–103

Yan B, Ren F, Cai M, Qiao C (2020) Bayesian model based on Markov chain Monte Carlo for identifying mine water sources in submarine gold mining. J Clean Prod 253:120008

Yang L, Wang Q, Liu X (2015) Correlation between mineralization intensity and fluid–rock reaction in the Xinli gold deposit, Jiaodong Peninsula, China: constraints from petrographic and statistical approaches. Ore Geol Rev 71:29–39

Yang L, Zhao R, Wang Q, Liu X, Carranza E (2018) Fault geometry and fluid-rock reaction: combined controls on mineralization in the Xinli gold deposit, Jiaodong Peninsula, China. J Struct Geol 111:14–26

Yang J, Dong S, Wang H, Li G, Wang T, Wang Q (2020) Mine water source discrimination based on hydrogeochemical characteristics in the northern Ordos Basin, China. Mine Water Environ. https://doi.org/10.1007/s10230-020-00723-5

Zhang H, Yao D (2020) The Bayes recognition model for mine water inrush source based on multiple logistic regression analysis. Mine Water Environ 39:888–901

Zhao H, Ma F, Li G, Zhang Y, Guo J (2012) Study of the hydrogeological characteristics and permeability of the Xinli seabed gold mine in Laizhou Bay, Jiaodong Peninsula, China. Environ Earth Sci 65(7):2003–2014

Zhao R, Liu X, Pan R, Zhou M (2015) Element behaviors during alteration and mineralization: a case study of the Xinli (altered rock type) gold deposit, Jiaodong Peninsula. Acta Petrol Sin 31(11):3420–3440